Organ Surface Deformation Measurement and Analysis in Open Hepatic Surgery: Method and Preliminary Results From 12 Clinical Cases

Logan W. Clements*, Prashanth Dumpuri, William C. Chapman, Benoit M. Dawant, *Member, IEEE*, Robert L. Galloway, *Member, IEEE*, and Michael I. Miga, *Member, IEEE*

***Abstract*—The incidence of soft tissue deformation has been well documented in neurosurgical procedures and is known to compromise the spatial accuracy of image-guided surgery systems. Within the context of image-guided liver surgery (IGLS), no detailed method to study and analyze the observed organ shape change between preoperative imaging and the intraoperative presentation has been developed. Contrary to the studies of deformation in neurosurgical procedures, the majority of deformation in IGLS is imposed prior to resection and due to laparotomy and mobilization. As such, methods of analyzing the organ shape change must be developed to use the intraoperative data [e.g., laser range scan (LRS) surfaces] acquired with the organ in its fully deformed shape. To achieve this end we use a signed closest point distance deformation metric computed after rigid alignment of the intraoperative LRS data with organ surfaces generated from the preoperative tomograms. The rigid alignment between the intraoperative LRS surfaces and preoperative image data was computed with a feature weighted surface registration algorithm. In order to compare the deformation metrics across patients, an interpatient nonrigid registration of the preoperative CT images was performed. Given the interpatient liver registrations, an analysis was performed to determine the potential similarities in the distribution of measured deformation between patients for which similar procedures had been performed. The results of the deformation measurement and analysis indicate the potential for soft tissue deformation to compromise surgical guidance information and suggests a similarity in imposed deformation among similar procedure types.**

***Index Terms*—Image-guided surgery (IGS), laser range scanning, open hepatic surgery, soft tissue deformation.**

Manuscript received December 8, 2009; revised April 8, 2010 and July 14, 2010; accepted July 14, 2010. Date of publication April 25, 2011; date of current version July 20, 2011. This work was supported by the National Institute of Biomedical Imaging and Bioengineering, the National Institutes of Health, NIH R21, under Grant EB 007694-01. *Asterisk indicates corresponding author.*

*L. W. Clements was with the Department of Biomedical Engineering, Vanderbilt University, Nashville, TN, 37215 USA. He is now with Pathfinder Therapeutics, Inc., Nashville, TN, 37204 USA (e-mail: loganc@pathsurg.com).

P. Dumpuri, R. L. Galloway, and M. I. Miga are with the Department of Biomedical Engineering, Vanderbilt University, Nashville, TN, 37215 USA (e-mail: prashanth.dumpuri@vanderbilt.edu; bob.galloway@vanderbilt.edu; michael.i.miga@vanderbilt.edu).

W. C. Chapman is with the Department of Surgery and Cell Biology, Section of Transplantation, Washington University School of Medicine, St. Louis, MO 63110 USA (e-mail: chapmanwi@wudosis.wustl.edu).

B. W. Dawant is with the Department of Electrical Engineering and Computer Science, Vanderbilt University, Nashville, TN 37215 USA (e-mail: benoit.dawant@vanderbilt.edu).

Color versions of one or more of the figures in this paper are available online at http://ieeexplore.ieee.org.

Digital Object Identifier 10.1109/TBME.2011.2146782

I. Introduction

THE goal of image-guided surgery (IGS) is to use preoperatively acquired tomographic images interactively within the surgical setting. Commercial IGS systems have been used in neurosurgical procedures for over a decade and are currently emerging for use in open abdominal procedures. More specifically, IGS techniques have been proposed for use in open hepatic resection procedures where minimizing the resection of healthy tissue is of vital importance for ensuring sufficient remnant liver volume [1]–[3]. Additionally, IGS technology presents value in obtaining sufficient resection margin and avoiding important vascular structures in hepatic procedures where nonanatomical wedge resections are performed.

A critical component of IGS devices is the performance of a mathematical mapping, or registration, of the intraoperative presentation to the preoperative image data. A significant body of work has been dedicated to exploring methods to provide this registration within the context of open hepatic procedures [2]–[5], allowing for the realization of an image-guided liver surgery (IGLS) [1]. However, the *de facto* methods of obtaining the image-to-physical space registration for IGLS have required the use of rigid body assumptions. These assumptions are known to be invalid due to the incidence of soft tissue deformation. For example, brain deformations (commonly referred to as "brain shift") have been well documented within the literature and have been shown to compromise the guidance information provided by commercially available neurosurgical IGS systems [6]–[9]. The registration error resulting from soft tissue deformation in image-guidance technologies limits their utility during the procedure by rendering inaccurate surgical position overlays on the preoperative image data.

Unfortunately, the measurement techniques applicable within the neurosurgical context such as the tracking of cortical features do not translate to IGLS readily since a large component of the observed liver deformation does not have a time varying component. Within this study we will rely on the use of intraoperatively obtained laser range scan (LRS) data of the liver surface acquired after the performance of laparotomy and liver mobilization. While it is clear the deformation measurements with respect to subsurface structures would be highly relevant, this initial work focuses on surface deformation measurements. This is due to fact that the ability to accurately localize subsurface targets intraoperatively via tracked ultrasound or intraoperative CT were not available.

Due to the nature of open hepatic procedures, in contrast to neurosurgery, the majority of deformation occurs before the acquisition of surface data via LRS is possible. Since distinct features are not present within IGLS, new techniques of visualization and analysis to properly understand the nature of the shape change experienced in open hepatic procedures have been developed. The primary intent of this study is to provide an indication of the range of surface deformations encountered during open IGLS over a variety of surgical procedures. Measuring the extent of deformation encountered in open hepatic surgery over a variety of surgical procedures will provide insight into the magnitude of spatial inaccuracy experienced during IGLS.

A. Related Work

While a number of techniques have been proposed for the compensation of intraoperative deformation, a proper study of this behavior has not been performed within the context of IGLS. As mentioned previously, a number of studies have been performed to measure and analyze the brain shift encountered during neurosurgical procedures. Roberts *et al.* performed a quantitative analysis of cortical displacement in 28 cases by tracking specific features on the brain surface throughout the procedures [6]. Maurer *et al.* performed similar studies where point features on the brain surface were digitized with optical tracking system immediately upon durotomy and after performing functional mapping prior to resection [7], [8]. Additional studies were performed by Maurer et *al.* utilizing an interventional MR scanner to collect images throughout the surgical procedure [9].

The analysis of deformation for hepatic procedures has mainly been focused on the motion due to respiration. Cash et *al.* tracked the motion of a point on the liver surface due to respiration using an optically tracked pen probe during an open liver resection case [1]. A study by Shimizu *et al.* has been performed to analyze the motion of a liver tumor due to respiration via high-speed MR imaging to estimate potential errors associated with radiotherapy procedures [10]. Rohlfing *et al.* used gated, serial MR images to analyze respiratory motion via deformable registration methods [11]. More recently, a study performed by Heizmann *et al.* provided an assessment of intraoperative liver deformation using intraoperative computed tomography [12]. The results presented in this study focused more on intraoperative changes in segmental volumetrics rather than calculation of intraoperative displacements.

B. Objective

The objective of this study is to provide a measurement of the extent and nature of intraoperative soft tissue deformation encountered in open liver surgical procedures. Due to the nature of deformation in open hepatic procedures, intraoperative imaging can only be acquired after a majority of the deformation has occurred. In this study, we will provide a summary of surface deformation measurements over a range of surgical procedures. Additionally, the measured deformation was analyzed to determine the similarities between the measured deformations between similar resection procedures. The performance of this measurement and analysis provides insight into the nature of soft tissue deformation encountered in open hepatic procedures, which will likely facilitate the development of deformation compensation methods.

II. Methods

A. Patient Overview

Institutional Review Board (IRB) approval was obtained for the intraoperative acquisition of liver surface data as well as the use of the ORION surgical navigation system [13] at Barnes-Jewish Hospital in St. Louis, MO. A summary of the patient information for 12 of the cases performed between November 2004 and August 2006 for which intraoperative data was acquired is shown in Table I. Access to the clinical data used in this study can be made available on request (M. Miga).

B. Preoperative Image Acquisition and Processing

For each of the patients included in this study, CT image volumes were acquired approximately one week prior to performance of the surgical procedure (SOMATOM Sensation 64, Siemens Medical Solutions, Munich, Germany). A triphasic imaging protocol was employed for acquisition of arterial phase, venous phase, and noncontrast liver parenchymal tomographic volumes. The venous phase image sets, which capture the hepatic venous and portal venous structures in high contrast, were used for the analysis methods proposed in this study.

In order to facilitate the analysis of the intraoperative shape change, the organ surfaces for each of the cases must be generated from the preoperative image volumes. A semiautomatic method developed by Dawant *et al.* [14] Pan and Dawant [15], based on the level set method proposed by Sethian [16], was used to segment the liver from the surrounding anatomical structures in the preoperative tomograms. Isosurfaces were generated from the liver segmentations via the Marching Cubes Algorithm [17] and smoothed via radial basis functions (FastRBF toolkit, FarField Technology, Christchurch, NZ).

C. Intraoperative Surface Acquisition and Processing

The intraoperative surface data used for this study were acquired using an off-the-shelf LRS. The RealScan 200 C (3-D Digital Corporation, Bethel, CT) is capable of acquiring spatially dense 3-D point cloud surface representations of 500 lines per scene with as many as 512 samples per line and a spatial resolution on the order of 0.5 mm at the typical range acquired in this study (45–60 cm). In addition to the geometrical data, a digital image is also acquired of the scanners field of view. Via a predetermined calibration, the color data from the digital image can be texture mapped on the 3-D point cloud. A detailed validation of the imaging capabilities of the LRS system used has been provided by Sinha *et al.* [18] and Cash *et al.* [4]. The liver parenchyma was segmented from the raw LRS data and the FastRBF toolkit was used to provided a smooth, regularly sampled representation of the intraoperative surface. An example LRS dataset is shown in Fig. 1.

TABLE I
SUMMARY OF PATIENT INFORMATION INCLUDING THE PATHOLOGICAL AND SURGICAL DETAILS FOR THE CASES PERFORMED UNDER THE IRB PROTOCOL APPROVED AT BARNES-JEWISH HOSPITAL, ST. LOUIS, MO

Case	Age	Sex	Pathology	Surgical Procedure
1	42	F	T2 staged tumor in gallbladder fossa	Exploratory laparotomy including multiple wedge liver and peritoneal biopsies; no resection performed
2	75	M	T2 staged cholangiocarcinoma with positive cystic duct margin	Resection of extrahepatic bile duct and gallbladder bed including segments IV and V
3	67	M	Extensive hilar cholangiocarcinoma	Resection of extrahepatic biliary tree with bile duct tumor
4	81	M	Suspected gallbladder and bile duct cancer	Partial liver resection of IV-B and V with *en bloc* gallbladder resection; resection of extrahepatic bile ducts
5	51	F	Suspected left hilar cholangiocarcinoma	Multiple tumor biopsies with bi-lobar multifocal involvement in segments III, V, and VI; no resection performed
6	65	M	Cholagiocarcinoma involving left bile duct	Left hepatectomy with caudate lobe resection; resection of entire extrahepatic biliary tree
7	54	M	Metastatic chondrosarcoma in left lobe	Hepatic resection including segments II and III
8	49	F	Hilar cholangiocarcinoma in left lobe	Exploratory laparotomy including right lobe wedge biopsy; no resection performed
9	66	M	Metastatic colorectal carcinoma in right lobe	Right hepatectomy for removal of three foci
10	36	M	Hepatocellular carcinoma in left lobe	Left hepatectomy performed midway along segment IV for removal of tumor involving segments II and III with partial extension into segment IV
11	62	M	Metastatic colorectal cancer in right lobe	Exploratory laparotomy with multiple right lobe and intraperitoneal tumor biopsies
12	82	M	Metastatic colorectal cancer in segment VI	Resection of segment VI and wedge excision of segment V tumor

In accordance with the IRB protocol, the LRS data were acquired during preplanned apneic periods to minimize errors due to respiratory liver motion. The data were acquired at end expiration during the respiratory cycle, and the time within the surgical procedure where the surface data were acquired is summarized in Table II. In addition to the timing of data acquisition, the coverage of the scan data is also summarized.

To facilitate the interpatient deformation measurements within similar procedures, the patients were separated into three groups as noted in Table II. The three patients for which left hepatectomy procedures were performed were placed in Group A. The two patients that presented with left hilar cholangiocarcinoma, including bilobular and multifocal involvement, comprised Group B. The three patients for which right lobe biopsies and resections were performed comprised Group C. Finally, the patients placed in Group O did not fit in the aforementioned groups and were themselves different procedures. It should be noted that the data for patient 3 and patient 4 were excluded from the deformation analysis due to the lack of sufficient coverage of the acquired intraoperative LRS surface digitization.

D. Rigid Surface Registration of Intraoperative Data

Quantification of the surface deformation measured via the intraoperative LRS data relies on the ability to register this data with the liver surface generated from segmentation of the preoperative tomograms. To provide this registration we used the rigid surface salient feature registration algorithm developed previously [5]. The developed algorithm uses salient anatomical features that are easily identifiable in the preoperative tomogram and intraoperative LRS presentation and was inspired by the weighted geometrical features algorithm proposed by Maurer *et al.* [19]. The salient features used for the performance of the rigid surface regions in this study were the falciform ligament and inferior ridge along segments IV, V, and VI. An example of dataset highlighting the feature segmentations and the resulting salient feature preregistration is shown in Fig. 2.

As mentioned previously, the lack of surface coverage provided by the LRS data for patients 3 and 4 allowed the use of only a single patch region for the rigid surface registrations performed for these cases. In these registrations, only the falciform ligament or inferior ridge along segments IV, V, and VI was

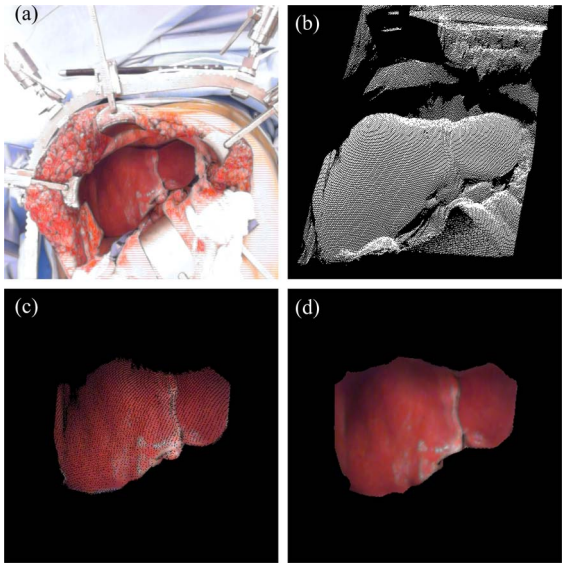

Fig. 1. Intraoperatively collected LRS dataset acquired for case 9. The texture map of the OR scene is shown in panel (a), the raw LRS point cloud is shown in panel (b), the segmented and texture mapped liver LRS surface data are shown panel (c), and panel (d) shows the RBF interpolation of the texture mapped liver surface shown in (c).

TABLE II
SUMMARY OF PATIENT INTRAOPERATIVE LRS ACQUISITION INCLUDING THE TIME OF THE SCAN AND THE SCAN COVERAGE

Case	Group	Scan Time	Coverage
1	O	post-laparotomy†	III-V,VIII
2	O	post-laparotomy†	II-V,VIII
3	N/A	pre-cholecystectomy	II-V,VIII
4	N/A	pre-cholecystectomy	III,IV
5	B	pre-cholecystectomy	II-V,VIII
6	A	post-cholecystectomy	II-V,VIII
7	A	post-laparotomy†	II-V,VIII
8	B	post-cholecystectomy	II-V,VIII
9	C	pre-cholecystectomy	III-V,VIII
10	A	pre-cholecystectomy	III-V,VIII
11	C	post-cholecystectomy	III-V,VIII
12	C	post-cholecystectomy	III-V,VIII

All of the scans were acquired prior to the performance of liver resection. Note that the data for patient 3 and patient 4 were not included in the deformation analysis studies due to the limited field of view obtained in the intraoperative LRS data.
†Patients with previously performed cholecystectomy.

used, and the surfaces were initially aligned using an anatomical fiducial point-based registration.

E. Interpatient Deformable Registration

In order to compare the measured intraoperative surface deformation across the 12 patients, it is necessary to compute an interpatient transformation between the preoperative CT image volumes. As the shape and volume of hepatic anatomy is highly variable between patients, a nonrigid image registration method is required. The adaptive basis algorithm (ABA) developed by Rodhe *et al.* was selected to provide the required

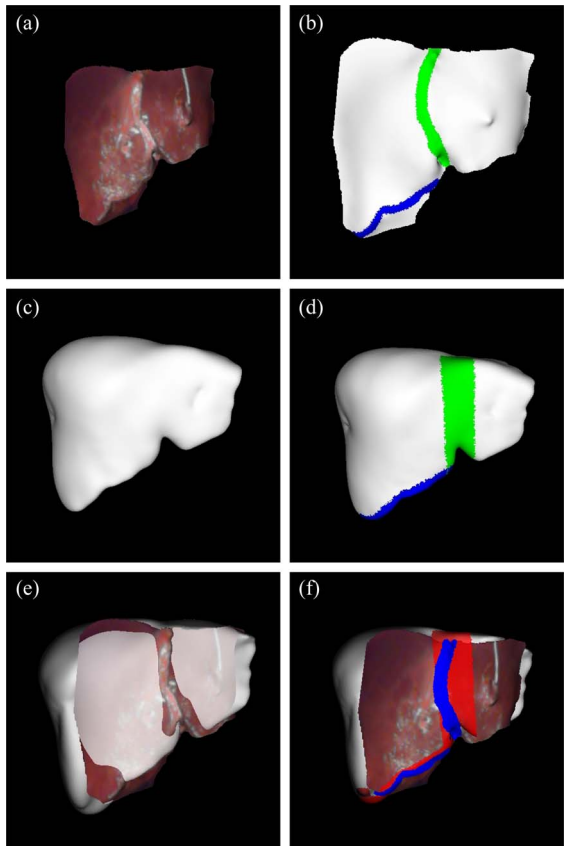

Fig. 2. LRS surface data (a)–(b), CT surface data (c)–(d) and resulting weighted patch ICP registration (e)–(f) for case 8. The segmentations of the patch regions are shown for the LRS and CT surfaces in panels (b) and (d), respectively. The falciform region is highlighted in green, while the inferior ridge of segments IV, V, and VI is shown in blue.

nonrigid transform for the intrapatient liver registration required for this study [20]. This algorithm has been used to perform interpatient brain registrations to create atlases for the placement of electrodes in deep brain stimulation procedures as well as to provide registrations between whole body images of mice for utilization in a variety of temporal and longitudinal studies [21]–[23].

Similar to the registration method proposed by Rueckert *et al.* [24], ABA employs a multiscale, multiresolution approach whereby the deformation field is modeled as the linear combination of a set of basis functions irregularly spaced over the image domain:

$$\mathbf{v}(\mathbf{x}) = \sum_{i=1}^{N} \mathbf{c}_i \mathbf{\Phi}(\mathbf{x} - \mathbf{x}_i) \tag{1}$$

where $\mathbf{x}$ is the coordinate vector in $\Re^d$ with d being the dimensionality of the image sets, $\mathbf{\Phi}$ is a Wu radial basis function with compact support [25], and $\mathbf{c}_i$ represents the coefficient weighting for each of these basis functions. The values of the coefficients are optimized such that the mutual information (MI) calculated between the deformed source and target images is maximized. For ABA, a steepest gradient descent optimization algorithm is used to solve for the optimal basis function coefficients.

To provide the initial alignment required for ABA, a surface-based registration was performed between the patient volumes via a rigid implementation of the iterative closest point (ICP) algorithm [26]. The surfaces were extracted from the segmented image volumes via the aforementioned segmentation and surface tessellation methods. Once transformed by the rigid transformation, the segmented source image volumes were then nonrigidly registered to the target volume via ABA. The ABA registration was implemented in a multilevel fashion with multiresolution and multiscale components similar to that described by Li *et al.* [21] Three image resolution levels were used for the interpatient liver registrations ($77 \times 77 \times 64$, $154 \times 154 \times 128$, and $308 \times 308 \times 255$), and the scale of basis functions used varied from a $3 \times 3 \times 3$ matrix for the lowest resolution to a $50 \times 45 \times 46$ matrix at the highest image resolution for a total of 15 levels. The parameters with regards to the multilevel approach were determined empirically.

For the purposes of this study, the segmented images were used to compute the interpatient liver registration due to anatomical differences with respect to gallbladder anatomy. The fact that some of the patients had prior cholecystectomies, while others presented with extremely distended gallbladders could confound the nonrigid registration algorithm and result in incorrect deformation fields in the neighborhood of the gallbladder fossa. The ABA registrations were performed such that all of the preoperative image volumes could be mapped to a single target space (i.e., patient 8 for this study), which facilitated the interpatient comparison of the distribution of measured deformation.

F. Tissue Deformation Metrics and Analysis

Given the rigid surface alignment of the intraoperative LRS and preoperative CT liver surfaces, the deformation analysis proceeded by computing the signed closest point distance values over the region of the preoperative image surface for which LRS data were acquired. The performance of point searches was used to facilitate the determination of both the region of liver covered by the LRS data and the Euclidean distance calculations. The directional sign for the distance value was determined by comparing the closest point distance vector with the surface normal. The closest point values were computed from target (i.e., CT liver surface) to source (i.e., LRS scan).

In addition to the signed closest point distance measurements, the displacement at the point of the umbilical fissure was calculated across all patient cases. The umbilical fissure is a groove on the inferior surface that holds the round ligament between segments III and IV. The round ligament is the only landmark that can be reliably identified in a retrospective manner in both the LRS and CT image data. To supplement the point displacement measurement, Euclidean closest point distance values were computed over the falciform and inferior ridge feature regions used in the salient feature surface registration algorithm.

Given the interpatient registration computed with the ABA algorithm, it is possible to compare the distribution of signed closest point distance measurements across patients to determine the correlation between the intraoperative surface deformation and surgical procedure. In order to compare the data across all patients, the regions of the liver surface for which LRS data existed over all cases had to first be computed. Note that we excluded two of the datasets (case 3 and case 4) from the computation of the overlap region due to insufficient LRS surface coverage. The correlation coefficient (CC) image similarity metric was chosen to compare the distribution of signed closest point distance measurements across patients. The CC metric is not biased by absolute differences in the underlying data and simply assumes a linear relationship. The CC value is determined via the following equation:

$$\mathrm{CC} = \frac{\sum_i \left(T(i) - \bar{T}\right)\left(S'(i) - \bar{S}'\right)}{\left[\sum_i \left(T(i) - \bar{T}\right)^2 \sum_i \left(S'(i) - \bar{S}'\right)^2\right]^{1/2}} \quad \forall\, i \in T \cap S' \qquad (2)$$

where S' is the transformed source dataset, T is the target dataset, and i represents the collection of overlapping surface points between the datasets. The mean deformation metric values in the transformed source and target datasets calculated for the overlap region are represented by $\bar{S}'$ and $\bar{T}$, respectively. Upon computation of the CC values between all permutations of patient comparisons, the CC values were averaged within the groups of patients for which similar procedures were performed ("in group"). For the purposes of comparison, CC average values were computed for the groups of patients for which the procedures were different ("out group").

III. Results

A. Rigid Surface Registration and Deformation Quantification

The results of the salient feature rigid surface registrations between the preoperative CT data and intraoperative LRS liver surfaces for the cases included in Groups A, B, and C are shown in Figs. 3–5, respectively. Additionally, the computed signed distance measurements using the rigid surface registration are texture mapped on the preoperative image surfaces to provide a qualitative visualization of the observed deformations over the particular groups of cases. A summary of the signed closest point distances for all clinical cases, the feature error measurements, and the point displacement measured at the umbilical fissure are shown in Table III, which indicates the range of intraoperative surface shifts imposed in open hepatic procedures.

The surface deformation measurements summarized in Table III indicate that the range of point displacement magnitudes is from approximately 0.5 to 2 cm. Additionally, the range of closest point distance measurements have magnitudes from approximately 1 to 2 cm. These ranges represent considerable shape change between the preoperative image and intraoperative presentation.

When comparing the deformation measurements in Table III in terms of the presence or absence of the gallbladder based on Table II, there seems to be no clear trend. Intuitively, it seems as though scan data acquired precholecystecomy or in patients where the gallbladder had been previously removed would result

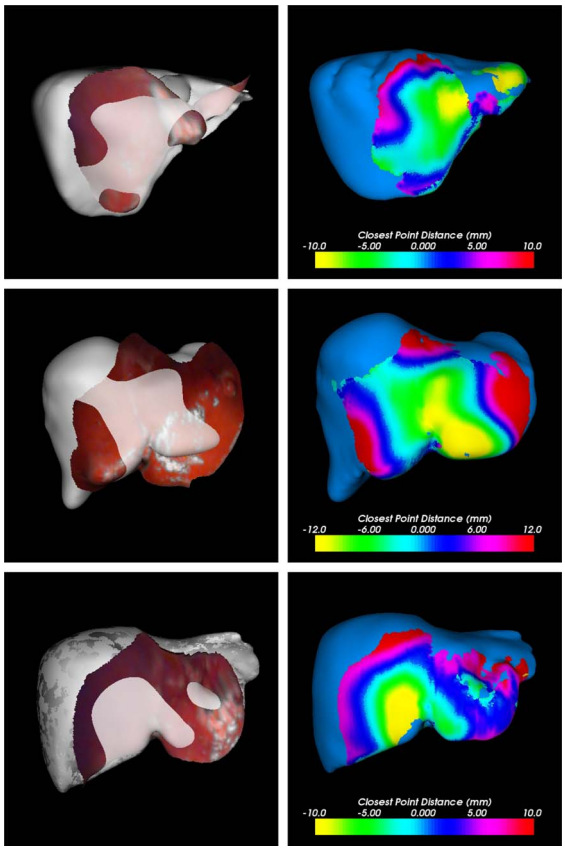

Fig. 3. Visualizations of the results of the rigid surface registration (left column) for the three group A cases (i.e., left hepatectomies). The signed distance (right column) values texture mapped on the preoperative surfaces are also shown. For reference, the visualizations for case 6, case 7, and case 10 are shown in the top, middle, and bottom rows, respectively.

in generally lower deformation measurements, but this generally does not seem to be the case.

The signed distance distributions for the left hepatectomy cases (Group A), as shown in the right column of Fig. 3, seem to display a similar pattern in the distribution of deformation. The pattern of the deformation across the Group A patients, where the central scan region is the location of a majority of the negative closest point distances and the peripheral scan regions lie above the preoperative surface, indicates an overall flattening of the surface in the intraoperative presentation. It should be noted that the overall shape change indicted by the signed closest point distance distribution for Group A is very similar to that for the Group C cases, as shown in Fig. 5. However, the region where a majority of the flattening of the organ is evident seems to be shifted closer to the left lobe for the Group A cases and toward the right lobe of the liver for the Group C cases.

While the general pattern of shape change with regards to the signed closest point distance distribution for the left hilar cholangiocarcinoma patients (Group B) is markedly different than the qualitative results shown for Group A and Group B, the "in group" similarity of the metric distribution is evident. The peripheral scan regions for the Group B cases yield negative closest point distances since the intraoperative LRS data lie below the preoperative surface. This seems to indicate a sub-

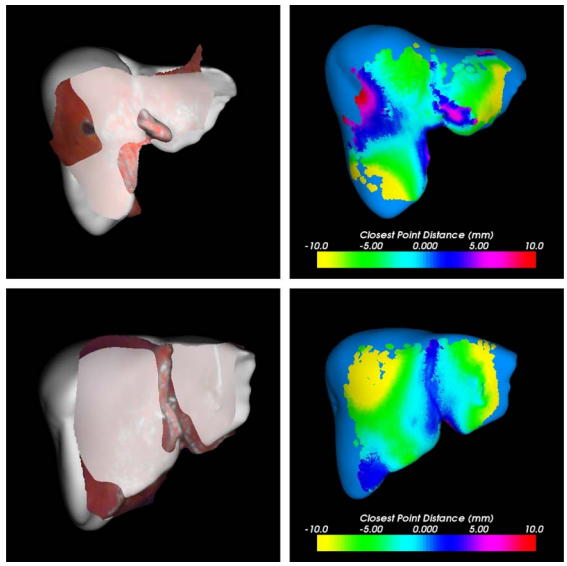

Fig. 4. Visualizations of the results of the rigid surface registration (left column) for the two group B cases (i.e., left hilar cholangiocar-cinoma with bilobular, multifocal involvement). The signed distance (right column) values texture mapped on the preoperative surfaces are also shown. For reference, the visualizations for case 5 and case 8 are shown in the top and bottom rows, respectively.

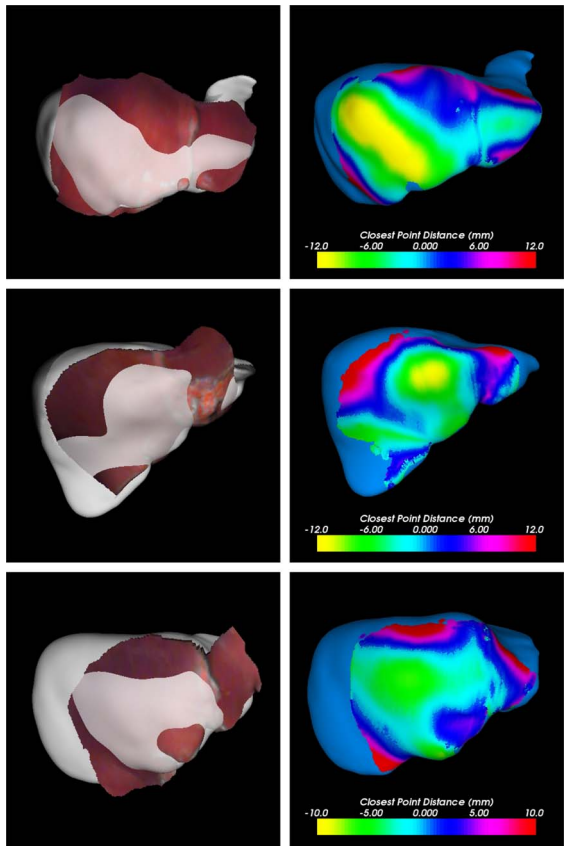

Fig. 5. Visualizations of the results of the rigid surface registration (left column) for the three group C cases (i.e., right lobe biopsies and resections). The signed distance (right column) values texture mapped on the preoperative surfaces are also shown. For reference, the visualizations for case 9, case 11, and case 12 are shown in the top, middle, and bottom rows, respectively.

TABLE III
COMPREHENSIVE SUMMARY OF THE SIGNED CLOSEST POINT DISTANCE, FEATURE ERROR, AND SINGLE POINT DISPLACEMENT MEASUREMENTS OVER THE 12 CLINICAL CASES

Group	Patient	Closet Point Measurements			Target Error Measurements		
		Mean±St.d.	Median	Range (Max,Min)	Feature 1 Mean±St.d. (Max)	Feature 2 Mean±St.d. (Max)	Point
A	6	-1.2±4.5	-1.4	(14.1,-13.9)	N/A	1.6±1.0 (4.7)	5.9
A	7	1.6±8.4	0.8	(22.9,-16.4)	4.5±2.9 (14.0)	2.0±1.7 (8.3)	15.9
A	10	1.4±5.3	2.0	(19.5,-15.6)	2.8±1.6 (9.4)	6.5±3.4 (18.9)	13.6
B	5	-2.6±4.7	-2.7	(12.8,-18.8)	2.5 ± 1.7 (6.6)	2.5 ± 2.0 (11.5)	6.9
B	8	-3.9±4.3	-3.3	(9.3,-15.2)	2.1±1.3 (7.0)	1.2±0.6 (3.4)	5.1
C	9	-1.3±6.2	-1.3	(18.9,-13.6)	2.8±2.5 (8.9)	2.2±1.2 (6.5)	16.8
C	11	0.1±5.5	-0.7	(18.6,-12.5)	2.4±2.8 (14.6)	3.8±2.2 (9.1)	7.4
C	12	0.7±4.73	-0.4	(19.6,-7.6)	1.8±0.8 (4.3)	2.6±1.3 (11.1)	5.2
O	1	-1.3±4.2	-2.0	(18.2,-9.4)	2.0±1.2 (7.1)	2.3±2.7 (17.0)	11.1
O	2	0.7±3.4	0.8	(12.1,-7.6)	3.1±1.7 (8.5)	2.9±2.3 (9.0)	9.1
N/A	3	-0.8±4.9	-1.9	(19.7,-19.8)	3.7±1.8 (7.5)	2.5±1.6 (6.1)	10.3
N/A	4	-0.6±4.3	-0.7	(8.4,-10.9)	N/A	1.7±1.3 (5.6)	12.5

The single point displacement error was evaluated at the umbilical fissure. The values of mean, standard deviation, median, and range of distance measurements are reported in mm units. The range of surface error measurements indicates surface displacements on the order of 0.5 to 2 cm.

stantially different change in the overall organ shape for the Group B patients as compared with the other groups. Generally speaking, the intraoperative surface seems to be generally more curved and less flat than the preoperative organ shape.

As mentioned, the general distribution of the signed closest point measure of deformation for the Group C cases indicates a qualitative similarity in the organ shape change for the right lobe biopsy and resection procedures. While the magnitude of the measured dis- tances varies within the patient group, signed distance distribution indicates a generally flattening of the organ as in the Group A cases. The difference between the observed organ shape change in Group C, as compared with the Group A cases, is the shift to the right of the region of negative closest point distances. The difference in the location of the flattening shape change is due, presumably, to the differences in the mobilization methods used for these procedures. Overall, the visualizations of the distribution of signed closest point distance indicate a general similarity within the patient groups. While the absolute magnitudes of the distances are different with each group there seems to be a general similarity in the nature of the deformation.

TABLE IV
SUMMARY OF INTERPATIENT DEFORMABLE REGISTRATION VALIDATION IN TERMS OF CLOSEST POINT DISTANCE VALUES

SRC Case	TAR - Case 8 SRC→TAR Mean±St.d.	SRC→TAR Max	Overlap Mean±St.d.	Overlap Max
1	0.9±0.5	6.1	0.9±0.4	2.8
2	1.2±0.6	5.0	1.1±0.5	2.6
3	0.9±0.6	16.0	N/A	N/A
4	1.1±1.1	22.7	N/A	N/A
5	1.8±1.1	15.4	1.0±0.6	3.3
6	1.1±0.8	17.3	1.0±0.4	3.2
7	1.0±0.5	6.9	0.8±0.3	2.0
9	2.2±5.5	57.1	0.9±0.4	2.5
10	0.9±0.9	24.4	0.8±0.29	2.1
11	0.8±0.4	5.0	0.7±0.3	2.4
12	0.9±0.4	4.8	0.7±0.3	1.9

These values were calculated both from the transformed source (SRC) surface to the target (TAR) surface and from the TAR to SRC surface. Additionally, the closest point distance values were reported as averages over the entire surface and over the region of overlap for which LRS data existed across all patients (shown in last two columns). Note that the maximum closest point distance values were significantly lower in the overlap region as compared with the entire surface.

B. Interpatient Deformable Registration

The results of the interpatient deformable registrations provided by ABA are summarized in Table IV to verify that the method provides registrations that are of sufficient accuracy for use in deformation distribution comparison across the patient population. A qualitative visualization of registration result for a single case in terms of surface renderings is shown in Fig. 6. Overall, the closest point distance measurement of error suggests that the registration results are of sufficient accuracy to be viable for use the proposed interpatient deformation comparison. The largest errors reported in Table IV were for the registration performed for case 9, which was due to the presence of an atypical anatomical extension of liver parenchyma visible at the left lateral segment, which was not present in the target liver (i.e., case 8) or any other dataset. Furthermore, it should be noted that the closest point distance measure of errors was much smaller when averaged over the region of LRS data overlap as compared with the average computed over the entire surface. This seems to indicate that the registration errors are minimal in the region where the interpatient comparison of the deformation was to be performed.

Given the ABA interpatient registration results, the computed overlap region for the ten included datasets mapped on the target liver surface is shown in Fig. 7. It is over this region that the interpatient comparison of measured surface deformation was performed.

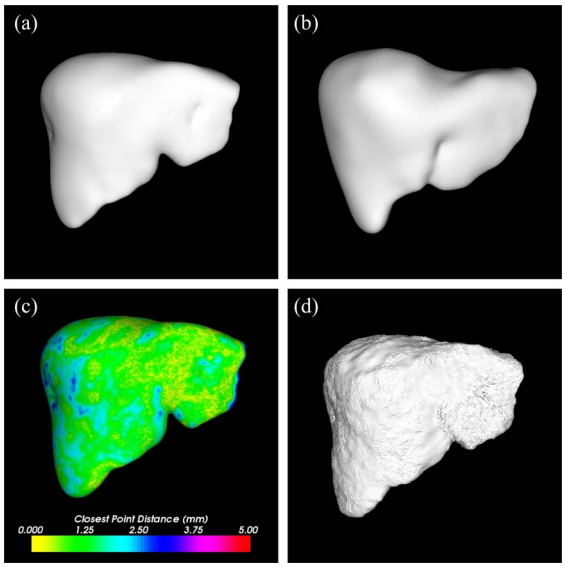

Fig. 6. Example result of the interpatient deformable registration between case 2 (source) and case 8 (target). The target and source surfaces for case 8 and case 2 are shown in panels (a) and (b), respectively. The transformed source surface is shown in panel (d), and the closest point distances between the target and transformed source surfaces textured mapped on the target surface is shown in panel (c). A numerical summary of the visualized deformable registration result in terms of closest point surface distances can be found in Table IV.

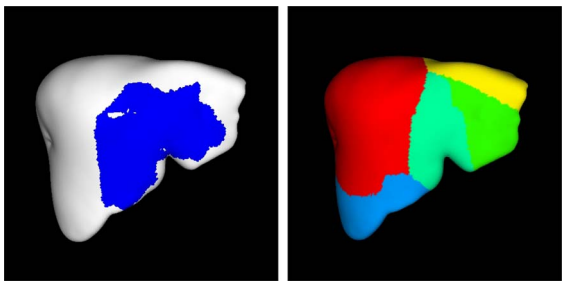

Fig. 7. Display of the overlap region (left panel) calculated via the interpatient registration on the target image surface. The overlap region contained 5065 points and contained measurements within segments II, III, IV, V, and VI. The right panel shows the Couinaud segment delineation for the patient provided by MeVis Medical Solutions (Bremen, Germany).

C. Summary of the Deformation Analysis

The CC values were computed between all the cases over the computed overlap region (shown in Fig. 7) for the signed distance deformation measurements. In order to determine the similarity in measured deformation between similar surgical procedures, the mean CC values were then computed within the three groups of clinical cases (i.e., "in group" mean). The mean CC values computed for the signed distance measurements over the three patient groups are shown in Table V.

Similar to the qualitative visualizations, analysis of mean CC values computed for the signed distance deformation measurement shows marked evidence of a correlation in the imposed organ shape change within similar procedures. While the small number of patient cases impedes the ability to make strong statistical conclusions, the absolute magnitude of the difference between the "in group" and "out group" CC means for the signed distance measure implies a similarity in the imposed deformation among similar procedure types.

TABLE V
SUMMARY OF THE COMPARISONS OF THE CC CALCULATIONS FOR THE SIGNED DISTANCE MEASUREMENTS MADE FOR THE OVERLAPPED SURFACE REGION

Group	In-Group	Out-Group
A	0.23±0.24	-0.09±0.32
B	0.35	-0.11±0.27
C	0.40±0.08	0.00±0.37

For each patient group, "in-group" and "out-group" mean CC values are shown.

IV. DISCUSSION

The surface deformation measurement study performed indicates that the surface displacements occur with magnitudes and 0.5 to 2.0 cm and maximum closest point distance magnitudes from approximately 1.0 to 2.0 cm. Generally, the shape change that occurs from preoperative image acquisition to intraoperative presentation involves a substantial flattening of the liver. The time of scan acquisition with respect to the performance of cholecystectomy does not seem to play a substantial role in the soft tissue deformation. While the surface deformation measurements give an indication that there is a substantial organ shape change encountered in open hepatic procedures, it is unclear how these surface errors translate into errors observed with respect to deep tissue structures. As mentioned, the modalities of tracked ultrasound and intraoperative CT were not available for this study, but future work should include such subsurface error measurements for a more complete description of soft tissue deformation in open hepatic procedures.

A qualitative comparison of the distribution of deformation suggests similarity in the shape change among similar surgical procedures presumably due to the patterns of mobilization and liver positioning per procedure type. Additionally, the proposed analysis suggests that there is a correlation in the distribution of the signed closest point distance measure of intraoperative deformation within groups of similar surgical procedures. The fact that similar deformation patterns are reflected among similar resection procedures provides a very powerful insight into potential solutions for the compensation for soft tissue deformation in IGLS.

The qualitative visualizations and quantitative measurements of intraoperative surface deformation experienced in open hepatic procedures suggest that the guidance information provided by IGLS can be compromised to a substantial degree by soft tissue deformation. The proposed methods to compensate for soft tissue deformation in IGLS have primarily been to use the forward solution of finite element modeling (FEM) liver models using a driving force computed via sparse intraoperative data [27], [28]. A number of other groups have focused on deformable registration techniques using B-spline interpolation to warp to the preoperative images to the intraoperative ultrasound acquisitions [29]–[31]. A common theme with these proposed methods is the incurred user interaction for boundary

condition and material property specification required to execute the algorithms during the surgical procedure.

Given the similarity in deformation measured between similar surgical procedures in open hepatic surgery, it may be reasonable to use an atlas shape-based approach wherein an array of FEM solutions are computed with preoperatively given the *a priori* information regarding the surgical procedure. Within such a technique a number of preoperatively computed solutions would be generated with varying material properties as well as a range of reasonable boundary conditions, given knowledge of the typical deformation distributions for a particular procedure type. Similar deformation compensation methods have been proposed by Davatzikos *et al.* [32] and Mohamed *et al.* [33]. More recently, Mohamed *et al.* expanded the atlas-based technique proposed for brain image applications to include tumor-induced deformations [34]. Additionally, a promising atlas-based technique has been proposed for model updating in image-guided neurosurgery by Dumpuri *et al.* [35]. A preliminary study has been conducted to make these methods amenable to IGLS deformation compensation [36].

While the qualitative results of the deformation analysis seem to suggest a correlation between the imposed deformation and the surgical procedure, it is important to note that all of the data acquired was for surgeries performed by a single surgeon (W. Chapman). It seems reasonable that the deformations imposed on the organ per procedure may vary based on the tendencies of the particular surgeon performing the procedure. A clinical trial by Pathfinder Therapeutics, Inc. (Nashville, TN), where LRS and other intraoperative digitizations are being acquired across three individual clinical sites (University of Pittsburg Medical Center, Memorial Sloan-Kettering Cancer Center, and Shands at University of Florida Cancer Hospital) is ongoing and will provide valuable data to supplement the findings reported here.

V. Conclusion

The measurement surface deformation within open hepatic procedures indicates that substation organ shape change is incurred intraoperative relative to the preoperative tomographic image data. Additionally, we have developed a protocol suitable for determining the extent that observed intraoperative surface deformation is correlated among similar surgical procedures. While a statistical comparison cannot be performed due to the limited sample size, a correlation between surgical procedure and the distribution of signed closest point distance measure of deformation seems quite likely. Finally, the impact of the individual surgeon with respect to surgical presentation of the organ, and the subsequent variations in deformation imparted, particularly with respect to subsurface structures, needs to be studied further.

Acknowledgment

The authors would like to thank Dr. Glasgow, Laflin, and Cstonos of Wash-ington University School of Medicine in St. Louis, MO, for their help in collecting the clinical range scan data used in this study. In addition, many of the algorithms and visualization tools used in this study were developed using the Visualization Toolkit (see http://www.vtk.org). The FastRBF Toolkit (FarField Technology, Christchurch, NZ) was used to generate a number of the surfaces shown. The ANN Nearest Neighbor Search Library (see http://www.cs.umd.edu/mount/ANN/) was used to speed up closest point searches. For disclosure, Dr. Chapman, Dr. Dawant, Dr. Galloway and Dr. Miga are founders and hold equity in Pathfinder Therapeutics, Inc., Nashville, TN.

References

[1] D. M. Cash, S. C. Glasgow, L. W. Clements, M. I. Miga, B. Dawant, Z. Cao, R. L. Galloway, and W. C. Chapman, "Concepts and preliminary data towards the realization of an image-guided liver surgery system," *J. Gastrointest. Surg.*, vol. 11, no. 7, pp. 844–859, Jul. 2007.

[2] A. J. Herline, J. L. Herring, J. D. Stefansic, W. C. Chapman, R. L. Galloway, Jr., and B. M. Dawant. (2000). Surface registration for use in interactive, image-guided liver surgery. *Comput. Aided Surg.*, [Online]. *5(1)*, pp. 11–17. Available: PM:10767091

[3] A. J. Herline, J. D. Stefansic, J. P. Debelak, S. L. Hartmann, C. W. Pinson, R. L. Galloway, and W. C. Chapman. (1999, June). Imageguided surgery: Preliminary feasibility studies of frameless stereotactic liver surgery. *Arch. Surg.* [Online]. *134(6)*, pp. 644–649. Available: PM:10367875

[4] D. M. Cash, T. K. Sinha, W. C. Chapman, H. Terawaki, B. M. Dawant, R. L. Galloway, and M. I. Miga, "Incorporation of a laser range scanner into image-guided liver surgery: Surface acquisition, registration, and tracking," *Med. Phys.*, vol. 30, no. 7, pp. 1671–1682, Jun. 2003.

[5] L. W. Clements, W. C. Chapman, B. M. Dawant, R. L. Galloway, and M. I. Miga, "Robust surface registration using salient anatomical features for image-guided liver surgery: Algorithm and validation," *Med. Phys.*, vol. 35, no. 6, pp. 2528–2540, Jun. 2008.

[6] D. Roberts, A. Hartov, F. Kennedy, M. Miga, and K. Paulsen, "Intraoperative brain shift and deformation: A quantitative analysis of cortical displacement in 28 cases," *Neurosurgery*, vol. 43, no. 4, pp. 749–758, Oct. 1998.

[7] C. R. Maurer, D. L. G. Hill, R. J. Maciunas, J. A. Barwise, J. M. Fitzpatrick, and M. Y. Wang, "Measurement of intraoperative brain surface deformation under a craniotomy," in *Medical Image Computing and Computer-Assisted Intervention—Miccai'98* (ser. Lecture Notes In Computer Science), 1998, vol. 1496, pp. 51–62.

[8] D. Hill, C. Maurer, R. Maciunas, J. Barwise, J. Fitzpatrick, and M. Wang, "Measurement of intraoperative brain surface deformation under a craniotomy," *Neurosurgery*, vol. 43, no. 3, pp. 514–526, 1998.

[9] C. R. Maurer, D. L. G. Hill, A. J. Martin, H. Y. Liu, M. McCue, D. Rueckert, D. Lloret, W. A. Hall, R. E. Maxwell, D. J. Hawkes, and C. L. Truwit, "Investigation of intraoperative brain deformation using a 1.5-T interventional mr system: Preliminary results," *IEEE Trans. Med. Imag.*, vol. 17, no. 5, pp. 817–825, Oct. 1998.

[10] S. Shimizu, H. Shirato, B. Xo, K. Kagei, T. Nishioka, S. Hashimoto, K. Tsuchiya, H. Aoyama, and K. Miyasaka, "Three-dimensional movement of a liver tumor detected by high-speed magnetic resonance imaging," *Radiother. Oncol.*, vol. 50, no. 3, pp. 367–370, Mar. 1999.

[11] T. Rohlfing, C. R. Maurer, W. G. O'Dell, and J. H. Zhong, "Modeling liver motion and deformation during the respiratory cycle using intensity-based nonrigid registration of gated MR images," *Med. Phys.*, vol. 31, no. 3, pp. 427–432, Mar. 2004.

[12] O. Heizmann, S. Zidowitz, H. Bourquain, S. Potthast, H.-O. Peitgen, D. Oertli, C. Kettelhack. (2010, Aug.). Assessment of intraoperative liver deformation during hepatic resection: prospective clinical study. *World J. Surg.* [Online]. *34(8)*, pp. 1887–1893. Available: http://dx.doi.org/10.1007/s00268-010-0561-x

[13] J. D. Stefansic, W. A. Bass, S. L. Hartmann, R. A. Beasley, T. K. Sinha, D. M. Cash, A. J. Herline, and R. L. Galloway, "Design and implementation of a PC-based image-guided surgical system," *Comput. Methods Programs Biomed.*, vol. 69, pp. 211–224, 2002.

[14] B. Dawant, S. Pan, and R. Li, "Robust segmentation of medical images using geometric deformable models and a dynamic speed function," in *Proc. Med. Image Comput. Comput.-Assist. Intervent. (MICCAI 2001)* (Lecture Notes in Computer Science, vol. 2208), pp. 1040–1047.

[15] S. Pan and B. M. Dawant, "Automatic 3D segmentation of the liver from abdominal CT images: A level-set approach," in *Medical Imaging 2001: Image Processing, Proc. SPIE*, vol. 4322, M. Sonka and K. Hanson, Eds., pp. 128–138.

[16] J. A. Sethian, *Level Set Methods and Fast Marching Methods: Evolving Interfaces in Computational Geometry, Fluid Mechanics, Computer Vision, and Materials Science*. Cambridge, U.K.: Cambridge Univ. Press, 1999.

[17] W. Lorensen and H. Cline, "Marching cubes: A high resolution 3D surface construction algorithm," *ACM Comput. Graph.*, vol. 21, no. 4, pp. 163–169, Jul. 1987.

[18] T. K. Sinha, B. M. Dawant, V. Duay, D. M. Cash, R. J. Weil, R. C. Thompson, K. D. Weaver, and M. I. Miga, "A method to track cortical surface deformations using a laser range scanner," *IEEE Trans. Med. Imag.*, vol. 24, no. 6, pp. 767–781, Jun. 2005.

[19] C. R. Maurer, G. B. Aboutanos, B. M. Dawant, R. J. Maciunas, and J. M. Fitzpatrick, "Registration of 3-D images using weighted geometrical features," *IEEE Trans. Med. Imag.*, vol. 15, no. 6, pp. 836–849, Dec. 1996.

[20] G. Rodhe, A. Aldroubi, and B. Dawant, "The adaptive bases algorithm for intensity based non rigid image registration," *IEEE Trans. Med. Imag.*, vol. 22, no. 11, pp. 1470–1479, Nov. 2003.

[21] X. Li, T. E. Yankeelov, T. E. Peterson, J. C. Gore, and B. M. Dawant, "Automatic nonrigid registration of whole body ct mice images," *Med. Phys.*, vol. 35, no. 4, pp. 1507–1520, Apr. 2008.

[22] P.-F. D'Haese, E. Cetinkaya, P. E. Konrad, C. Kao, and B. M. Dawant. (2005, Nov.). Computer-aided placement of deep brain stimulators: from planning to intraoperative guidance. *IEEE Trans. Med. Imag.* [Online]. *24(11)*, pp. 1469–1478. Available: http://dx.doi.org/10.1109/TMI.2005.856752

[23] P.-F. D'Haese, S. Pallavaram, K. Niermann, J. Spooner, C. Kao, P. E. Konrad, and B. M. Dawant, "Automatic selection of dbs target points using multiple electrophysiological atlases," in *Proc. Med. Image Comput. Comput. Assist Interv. Int. Conf. Med. Image Comput. Comput. Assist. Interv.*, 2005, vol. 8, no. Pt 2, pp. 427–434.

[24] D. Rueckert, L. I. Sonoda, C. Hayes, D. L. G. Hill, M. O. Leach, and D. J. Hawkes, "Nonrigid registration using freeform deformations: Application to breast mr images," *IEEE Trans. Med. Imag.*, vol. 18, no. 8, pp. 712–721, Aug. 1999.

[25] Z. M. Wu, "Multivariate compactly supported positive definite radial functions," *Adv. Comput. Math*, vol. 4, pp. 283–292, 1995.

[26] P. J. Besl and N. D. McKay, "A method for registration of 3-D shapes," *IEEE Trans. Pattern Anal. Mach. Intell.*, vol. 14, no. 2, pp. 239–256, Feb. 1992.

[27] M. Miga, D. Cash, Z. Cao, G. R. L., B. Dawant, and W. Chapman, "Intraoperative registration of the liver for image-guided surgery using laser range scanning and deformable models," in *Proc. SPIE Med. Imag.*, 2003, vol. 5029, pp. 350–359.

[28] D. M. Cash, M. I. Miga, T. K. Sinha, R. L. Galloway, and W. C. Chapman, "Compensating for intraoperative soft-tissue deformations using incomplete surface data and finite elements," *IEEE Trans. Med. Imag.*, vol. 24, no. 11, pp. 1479–1491, Nov. 2005.

[29] M. Nakamoto, H. Hirayama, Y. Sato, K. Konishi, Y. Kakeji, M. Hashizume, and S. Tamura. (2007, Oct). Recovery of respiratory motion and deformation of the liver using laparoscopic freehand 3d ultrasound system. *Med Image Anal.* [Online]. *11(5)*, pp. 429–442. Available: http://dx.doi.org/10.1016/j.media.2007.07.009

[30] J. M. Blackall, G. P. Penney, A. P. King, and D. J. Hawkes, "Alignment of sparse freehand 3-d ultrasound with preoperative images of the liver using models of respiratory motion and deformation," *IEEE Trans. Med. Imag.*, vol. 24, no. 11, pp. 1405–1416, Nov. 2005.

[31] T. Lange, S. Eulenstein, M. Hunerbein, H. Lamecker, and P. M. Schlag, "Augmenting intraoperative 3d ultrasound with preoperative models for navigation in liver surgery," in *Lecture Notes in Computer Science*, Ed., vol. 3217. Medical Image Computing and Computer-Assisted Intervention. New York: Springer-Verlag, 2004, pp. 534–541.

[32] C. Davatzikos, D. Shen, A. Mohamed, and S. Kyriacou, "A framework for predictive modeling of anatomical deformations," *IEEE Trans. Med. Imag.*, vol. 20, no. 8, pp. 836–843, Aug. 2001.

[33] A. Mohamed, C. Davatzikos, and R. Taylor, "A combined statistical and biomechanical model for estimation of intra-operative prostate deformation," in *Proc. 5th Int. Conf. Medical Image Computing and Computer-Assisted Intervention-Part II (MICCAI)*. London, U.K: Springer-Verlag, 2002, pp. 452–460.

[34] A. Mohamed, E. I. Zacharaki, D. Shen, and C. Davatzikos, "Deformable registration of brain tumor images via a statistical model of tumor-induced deformation," *Med. Image Anal.*, vol. 10, no. 5, pp. 752–763, Oct. 2006.

[35] P. Dumpuri, R. C. Thompson, B. M. Dawant, A. Cao, and M. I. Miga, "An atlas-based method to compensate for brain shift: Preliminary results," *Med. Image Anal.*, vol. 11, no. 2, pp. 128–147, 2007.

[36] L. W. Clements, P. Dumpuri, W. C. Chapman, R. L. Galloway, and M. I. Miga, "Atlas-based method for model updating in image-guided liver surgery," *Proc. SPIE*, vol. 6509, 650917, 2007; doi: 10.1117/12.710496.

Authors' photographs and biographies not available at the time of publication.